PERGAMON

Journal of Structural Geology 25 (2003) 515–528

JOURNAL OF STRUCTURAL GEOLOGY

www.elsevier.com/locate/jstrugeo

Discrete element modelling of contractional fault-propagation folding above rigid basement fault blocks

Emma Finch, Stuart Hardy*, Rob Gawthorpe

Basin and Stratigraphic Studies Group, Department of Earth Sciences, The University of Manchester, Manchester M13 9PL, UK

Received 17 July 2001; accepted 11 April 2002

Abstract

Many studies have shown that discrete (blind) faults at depth are commonly linked to more distributed deformation, in particular folding, at higher levels. One category of fault-related folds, forced folds, is common where there is a distinct mechanical contrast between faulted basement and sedimentary cover. Outcrop, numerical and analogue modelling studies indicate that such folds form as upward widening zones of distributed deformation (monoclines) above discrete faults at depth. With increasing displacement the folds are often cut by faults as they propagate upwards into the cover. While the trishear kinematic model of fault-propagation folding appears to approximately represent the geometric development of such structures, comparatively little is known of the mechanical controls on their development.

Here we present a 2D discrete element model of sedimentary cover deformation above a contractional fault in rigid basement. The elements consist of a series of soft spheres that obey Newton's equations of motion and initially interact with elastic forces under the influence of gravity. Particles are bonded until the separation between them exceeds a defined breaking strain at which time the bond breaks, simulated by the transition from repulsive–attractive forces to solely repulsive forces. The model is used to investigate the influence of basement fault dip and sedimentary cover strength on the geometry of the folds developed and the rate of fault propagation. In all cases an upward widening monocline occurs above the basement fault. We find that shallow basement fault dips produce homogenous thickening of the monocline limb while steeper dips produce contemporaneous thinning and thickening within the monocline. Thinning and thickening within the monocline are accommodated by a combination of small-scale faulting and folding. With decreasing cover strength, the zone of deformation becomes wider, localization does not occur on a single fault and fold geometries resemble trishear fold profiles with low propagation to slip ratios ($p/s \sim 1$). In contrast, a stronger cover produces a narrower zone of deformation, localization on a single fault and more rapid fault propagation (similar to trishear fold profiles where $p/s \sim 2-3$). The fault propagates into the cover at approximately the same angle as the basement fault. The model reproduces well many of the features observed in analogue modelling and reported from outcrop and seismic studies.

Keywords: Fault-propagation folding; Forced folds; Modelling; Fault tip

1. Introduction

Fault-propagation folds, and the blind faults that they are associated with, are of great interest from an academic point of view, where they have recently been recognized as extremely important for their seismic hazard potential (e.g. Shaw and Shearer, 1999; Allmendinger and Shaw, 2000) and for their importance in controlling stratigraphic architectures in sedimentary basins (e.g. Ford et al., 1997; Gawthorpe et al., 1997), and are also the location of many oil and gas traps (e.g. Mitra and Mount, 1998). They are found in both extensional and compressional settings, e.g. the Rhine Graben (Laubscher, 1982), the Gulf of Suez (Gawthorpe et al., 1997; Sharp et al., 2000), the North Sea (Withjack et al., 1988), the Laramide orogen (e.g. Erslev and Mayborn, 1997), the Bighorn and Uinta basins (Mitra and Mount, 1998) and the Californian peninsular ranges (e.g. Allmendinger and Shaw, 2000) (Fig. 1). Where a faulted rigid basement is involved in the deformation, the folds are often called 'forced' folds (Stearns, 1978; Withjack et al., 1990). Evidence from well-exposed folds with preserved growth strata (e.g. Gawthorpe et al., 1997) and from analogue (e.g. Withjack et al., 1990; Mitra and Islam, 1994) and numerical modelling (Haneberg, 1992, 1993; Patton and Fletcher, 1995; Cardozo et al., 2002; Johnson and Johnson, 2002a,b) has indicated that many fault-propagation folds form as upward

* Corresponding author. Tel.: +44-161-275-3773; fax: +44-161-275-3947.

E-mail address: shardy@fs1.ge.man.ac.uk (S. Hardy).

0191-8141/03/$ - see front matter © 2002 Elsevier Science Ltd. All rights reserved.
PII: S0191-8141(02)00053-6

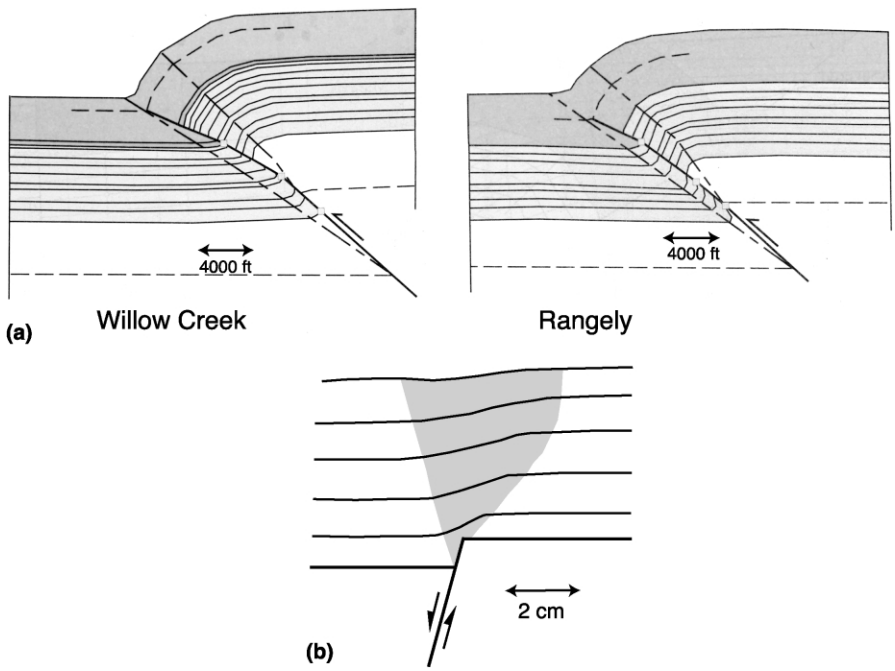

Fig. 1. (a) Natural examples of basement-involved structures: the Willow creek and Rangely anticlines (after Mitra and Mount, 1998), and (b) an analogue (clay) model of extensional fault-propagation folding (redrawn from Withjack et al., 1990)

widening zones of distributed deformation (monoclines) above discrete faults at depth. Field studies indicate that a variety of mechanisms are responsible for the distributed deformation including ductile flow, bedding slip, rigid rotation and small extensional and thrust faults (e.g. Gawthorpe et al., 1997; Sharp et al., 2000). Analogue modelling studies have shown that with increasing displacement (strain) the overlying fold may be cut by the fault as it propagates upwards into the cover. It has been suggested by Schlische (1995) and Hardy and McClay (1999) that the drag folds of some workers are in fact breached extensional fault-propagation folds. While these aspects of fault-propagation folds are reasonably well understood and documented (e.g. Erslev and Rogers, 1993; Schlische, 1995; Janecke et al., 1998; Mitra and Mount, 1998), and the trishear kinematic model appears to explain well their geometric development and finite strain (Erslev, 1991; Hardy and Ford, 1997; Allmendinger, 1998; Hardy and McClay, 1999; Zehnder and Allmendinger, 2000; Allmendinger and Shaw, 2000; Allmendinger et al., 2002), many aspects of their mechanics are unclear, e.g. What controls the geometry of the triangular shear zone? What influence does varying sedimentary cover strength have upon fault propagation and fold development? These and many other questions remain to be answered.

In an effort to better understand the development of such structures we have developed a 2D discrete element model (cf. Cundall and Strack, 1979) of sedimentary cover deformation in response to contractional basement faulting. The elements consist of a series of soft spheres which obey Newton's equations of motion and which initially interact with elastic forces under the influence of gravity. Faulting is simulated by the transition from repulsive–attractive forces between elements to solely repulsive forces. The model is used to investigate the influence of basement fault dip and sedimentary cover strength on the geometry of the fault-propagation folds that develop and the rate of fault propagation. We find that shallow basement fault dips produce thickening of the monocline limb while steeper dips produce contemporaneous thinning and thickening of stratigraphic units within the monocline. As the cover strength decreases, the zone of deformation becomes wider and fold geometries resemble trishear fold profiles with low p/s ratios, typically ~ 1. In contrast, a stronger cover produces a narrow zone of deformation and more rapid fault propagation (similar to trishear fold profiles where $p/s \sim 2$–3). The model produces many of the features seen both in outcrop examples and analogue modelling studies. In addition, we demonstrate that the trishear model is a good approximate representation of the kinematic behaviour of our models, and that the p/s ratio is a gross reflection of the strength of the cover.

2. 2D discrete element model

2.1. Method

The discrete element model used here, a development on that of Mora and Place (1993), is based on circular elements that interact in pairs as if connected by breakable elastic springs (Fig. 2a). The behaviour of the elements assumes that the particles interact through a 'repulsive–attractive' force (Mora and Place, 1993) in which the resultant force,

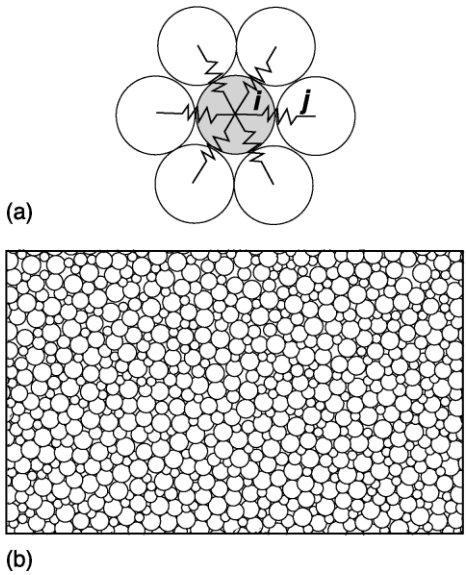

Fig. 2. Illustration of the discrete element technique used in the modelling discussed in this paper: (a) relationship between a given particle i and its α neighbours, particles are connected by breakable elastic springs, (b) packing of particles of four different radii used in this paper.

F_s, is given by:

$$F_S = \begin{cases} K(r-R), & r < r_o, \text{ intact bond} \\ K(r-R), & r < R, \text{ broken bond} \\ 0, & r \geq R, \text{ broken bond} \end{cases} \quad (1)$$

Here, K is the elastic constant (spring strength) of the bond, R is the equilibrium separation between the particles, and r is the current separation between the particle pair. Particles are bonded until the separation (r) between them exceeds a defined breaking strain, r_o, at which time the bond breaks. After this point, the particle pair experiences no further attractive force and the bond is irreversibly broken. However, if the two particles return to a compressive contact (i.e. $r < R$), a repulsive force acts between them. Healing of bonds is not permissible in the present model. In previous applications of this model, Mora and Place (1994) showed that breaking strains for most materials are typically much less than ~0.11, while the behaviour of particle assemblies in plane-strain compression tests under varying confining pressures and subject to different densities of pre-existing fractures was investigated by Donzé et al. (1994). The density of pre-existing fractures (or equivalently in our model the value of breaking strain) was found to control the intrinsic cohesion of the modelled material. Increasing the amount of pre-existing fractures results in a transition from brittle to ductile behaviour (see Donzé et al., 1994); we have confirmed that a decrease in the breaking strain from 0.1 to 0.01 in our models produces an analogous transition from brittle to ductile behaviour. In the model results reported here we investigate the effect of a range of values (0.01–0.1) of the breaking strain, with the breaking strain initially set to be $0.05R$.

The total elastic force, $F_{i,\alpha}$, exerted on a particle is obtained by summing the forces on each bond that links the particle to its α neighbours, calculated by:

$$F_{i,\alpha} = \sum_{j=1,\alpha} f_{i,j} \quad (2)$$

in which $f_{i,j}$ is the elastic force experienced by particle i from its neighbouring particle j. Additionally we include a viscous damping term which attenuates the high frequency dynamic features of the model, such as wave propagation (Donzé et al , 1994) and thermal fluctuations. Gravitational forces, F_g, acting on each element are calculated in the y direction. Therefore the total force on any particle is given by:

$$\vec{F} = F_{i,\alpha} - \nu\dot{x} + F_g \quad (3)$$

where ν represents the dynamic viscosity and $\dot{x}$ is the velocity of the particle.

At each discrete time step, the particles are advanced to their new positions within the model by integrating their equations of motion using Newtonian physics and a velocity-Verlat based scheme (Allen and Tildesley, 1987). The positions ($x(t)$) and velocities ($\dot{x}(t)$) of the particles at the next discrete time step ($t + \Delta t$), are calculated from:

$$x(t+\Delta t) = x(t) + \Delta\dot{x}(t) + \frac{\Delta t^2}{2!}\ddot{x}(t)$$
$$\dot{x}(t+\Delta t) = \dot{x}(t) + \frac{\Delta t}{2}(\ddot{x}(t) + \ddot{x}(t+\Delta t)) \qquad \ddot{x} = \frac{F(t)}{M} \quad (4)$$

In previous work, such discrete element simulations were carried out using a regular hexagonal lattice (where $\alpha = 6$). However, this imposed an unrealistic first-order geometric control in which the well-defined 60° planes of weakness in the lattice dominated the fault geometry of the resulting structure (e.g. Donzé et al., 1994). To counteract the influence of such isotropy, we generate a particle assembly in which the particles are distributed randomly and which consequently possesses no preferred planes of weakness (cf. Antonellini and Pollard, 1995; Scott, 1996). In the assembly used here four particle sizes of radii 0.5, 0.7, 0.9 and 1.0 lattice units are positioned at random in an enclosed rectangular box and allowed to settle under gravity until the void space is minimised. The equilibrium separation of a particle pair (i,j), $R_{i,j}$, in this random particle assembly is now defined as the distance between a particle and its neighbour (Fig. 2b).

2.2. Boundary and initial conditions

Here we apply this discrete element model to the problem of fault-propagation folding in a contractional setting in which the weaker cover is deformed in response to movement of a strong, rigid basement block. Our model is perhaps most appropriate to the re-activation of a pre-existing basement fault overlain by a younger un-faulted

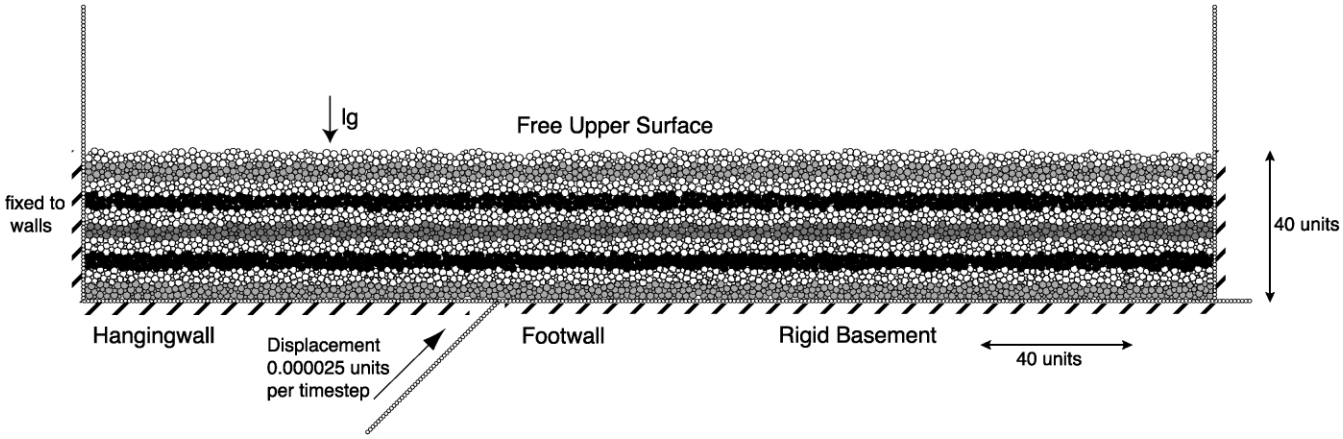

Fig. 3. Initial configuration of the standard model with a 45° fault in basement overlain by a cover which is initially unfaulted. A random lattice of 5925 particles is used. The values of the spring constant, K, and breaking strain used are 20 and 0.05R, respectively. The model is run for a total of 1,056,000 time steps, with at each time step 0.000025 units of displacement occurring along the basement fault, resulting in a total displacement of 26.4 units. The deformation is monitored with respect to 10 initially approximately flat-lying, constant-thickness beds. No vertical exaggeration.

sedimentary sequence. We use this model to investigate the influence of basement fault dip and sedimentary cover strength on the geometry of the folds developed, and the rates of fault propagation.

Within the basement we assume that there is a discrete pre-existing fault whose tip initially lies at the basement–cover interface, whereas in the cover there are no pre-existing faults (Fig. 3). We use a random lattice of 5925 particles to define the cover sequence, and assume that 1 lattice unit is 250 m and that the rock mass has a density of 2500 g/cm^3. Thus our particles represent the rock mass at a scale larger than a typical outcrop but the particle assembly is appropriate to major upper-crustal basement involved fault-related folds (cf. Fig. 1). The basement is assumed to be rigid (undeformable) and particles immediately overlying the basement are welded to it, as are particles adjacent to the sidewalls. We do not consider the mechanical properties of the basement material. The cover sequence is initially ca. 40 units thick. The values of the spring constant, K, breaking strain, and dynamic viscosity used are 20, 0.05R and 3.0, respectively, in our standard model. The effect of differing breaking strains is investigated later. The model is run for a total of 1,056,000 time steps, with at each time step 0.000025 units of displacement occurring along the basement fault, resulting in a total displacement of 26.4 units. As slip occurs on the basement fault the overlying cover sequence is deformed. The deformation is monitored with respect to 10 approximately flat-lying, constant-thickness marker beds; although we refer to these as 'beds' the cover is mechanically isotropic and layers are for visualization only.

3. Modelling of contractional fault-propagation folding above rigid basement fault blocks

In this section some examples of the structural relationships that are produced by the discrete element model described above are presented. In particular, the influence of two parameters on the geometries of the structures developed will be investigated: the dip of the basement fault and the mechanical strength of the sedimentary cover. For the initial and boundary conditions discussed in Section 2 we will present the sequential evolution of the following models: (a) basement fault dips of 30°, 45°, 60° and 80° for a model with a standard (0.05R) breaking strain, and (b) a range of cover breaking strains ranging from strong (0.10R), through standard (0.05R), weak (0.025R) and ultra-weak (0.01R) for the 45° basement fault dip model. Each model discussed takes approximately 90 h CPU time to run on a 40 processor SGI Origin 2000 supercomputer with a peak performance of 16 Gflops.

3.1. Basic evolution of model and influence of basement fault dip

Fig. 4 shows the sequential development of a model which has a basement fault dip of 45° and a breaking strain of 0.05R. This model will be used as the standard model against which the other models will be compared. The development of the model with increasing slip on the basement fault is shown after 330,000, 660,000, 858,000 and 1,056,000 timesteps (Fig. 4a–d). It can be seen that an upward-widening monocline forms above the discrete fault in basement; the monocline is slightly asymmetric with respect to the fault with somewhat more of the fold being located in the future hanging wall of the fault. Through time the limb of the monocline steepens and the fold becomes tighter with the final surface dip reaching approximately 25° (Fig. 4d). Within the monocline the dip of beds increases with depth and towards the fault tip. Individual beds (or groups of beds) show thinning (extensional faulting) in anticlinal regions and contemporaneous thickening (folding) in synclinal regions (Fig. 4d). As displacement

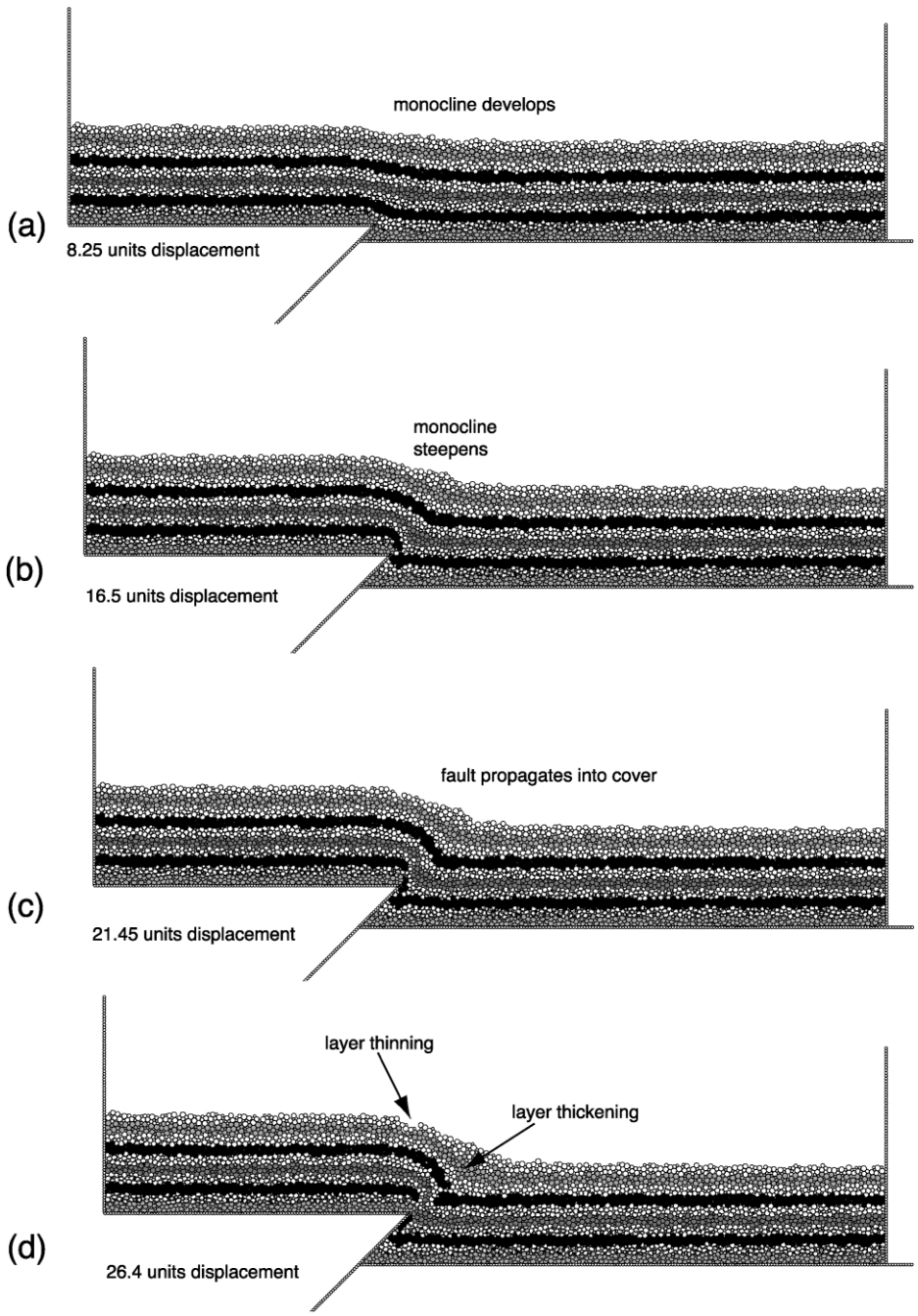

Fig. 4. Sequential evolution of the standard model with a basement fault dip of 45°. Configuration of the model is shown after (a) 330,000, (b) 660,000, (c) 858,000, and (d) 1,056,000 time steps. Total displacement applied is 26.4 units, all other parameters as in Fig. 3. For detailed methodology see text.

increases, the basement fault propagates up-section into the cover at an angle of approximately 45°. In doing so it can be seen to cut the overlying fold, producing a hanging wall anticline and footwall syncline on either side of the fault plane (Fig. 4d). These folds represent the breached monocline and are not the result of 'drag' adjacent to the fault plane (cf. Fig. 1a). Finally, however, the fault does not propagate through the entire thickness of the sedimentary cover.

Figs. 5–7 show the evolution of the standard model described above but with basement fault dips of 30°, 60° and 80°. All other model parameters are identical to those used in Fig. 4. In all models the structural evolution seen is broadly similar, with an upward-widening monocline developing initially but later steepening and being disrupted by a combination of folding and faulting. However, there are significant differences between the models that are a direct result of changing basement fault dip: a decrease in basement fault dip clearly leads to more homogenous thickening (in the form of small-scale folding) of the monocline limb and a small amount of extensional faulting (Fig. 5). The zone of deformation is still broadly triangular

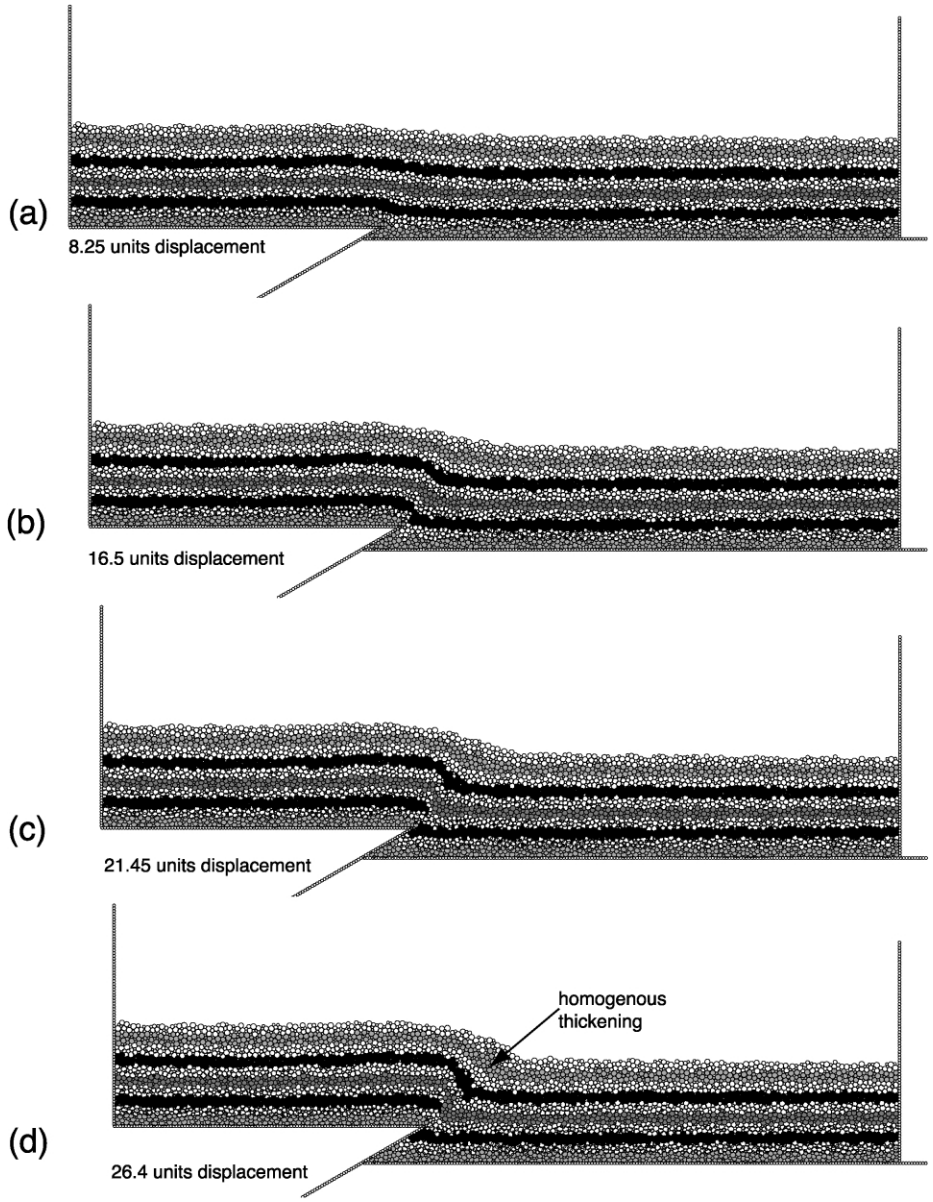

Fig. 5. Sequential evolution of a model with a basement fault dip of 30°. Configuration of the model is shown after (a) 330,000, (b) 660,000, (c) 858,000, and (d) 1,056,000 time steps. Total displacement applied is 26.4 units, all other parameters as in Fig. 3. For detailed methodology see text.

and focussed on the basement fault tip. In contrast, it can be seen that the effect of increasing basement fault dip is to increase the amount of extensional faulting within the monocline particularly in the region of the anticlinal hinge (compare Figs. 4d, 6d and 7d). This is particularly clear in the model with a basement fault dip of 80° (Fig. 7) where contemporaneous extensional faulting in the anticlinal hinge region and folding in the thickening synclinal hinge region occurs.

3.2. Influence of sedimentary cover strength

In this section we investigate the influence of sedimentary cover strength on the evolution of folding and faulting within the model. This is done by comparing a series of models with weaker and stronger cover strengths (expressed in terms of their breaking strain) to the standard 45° model with a breaking strain of $0.05R$ discussed in the previous section. Mora and Place (1994) showed that breaking strains for most materials are typically much less than ~0.11 and here we consider breaking strains in the range 0.01–0.10. Fig. 8 shows the sequential evolution of a model with weaker sedimentary cover (breaking strain reduced to $0.025R$) whereas Fig. 9 shows the evolution of a model with stronger sedimentary cover (breaking strain increased to $0.10R$). Fig. 10 shows the evolution of a model with an ultra-weak sedimentary cover (breaking strain reduced to $0.01R$). These figures show that there are major differences in the structures developed in the cover; examination of the models indicates that weaker cover strength results in: (a) a

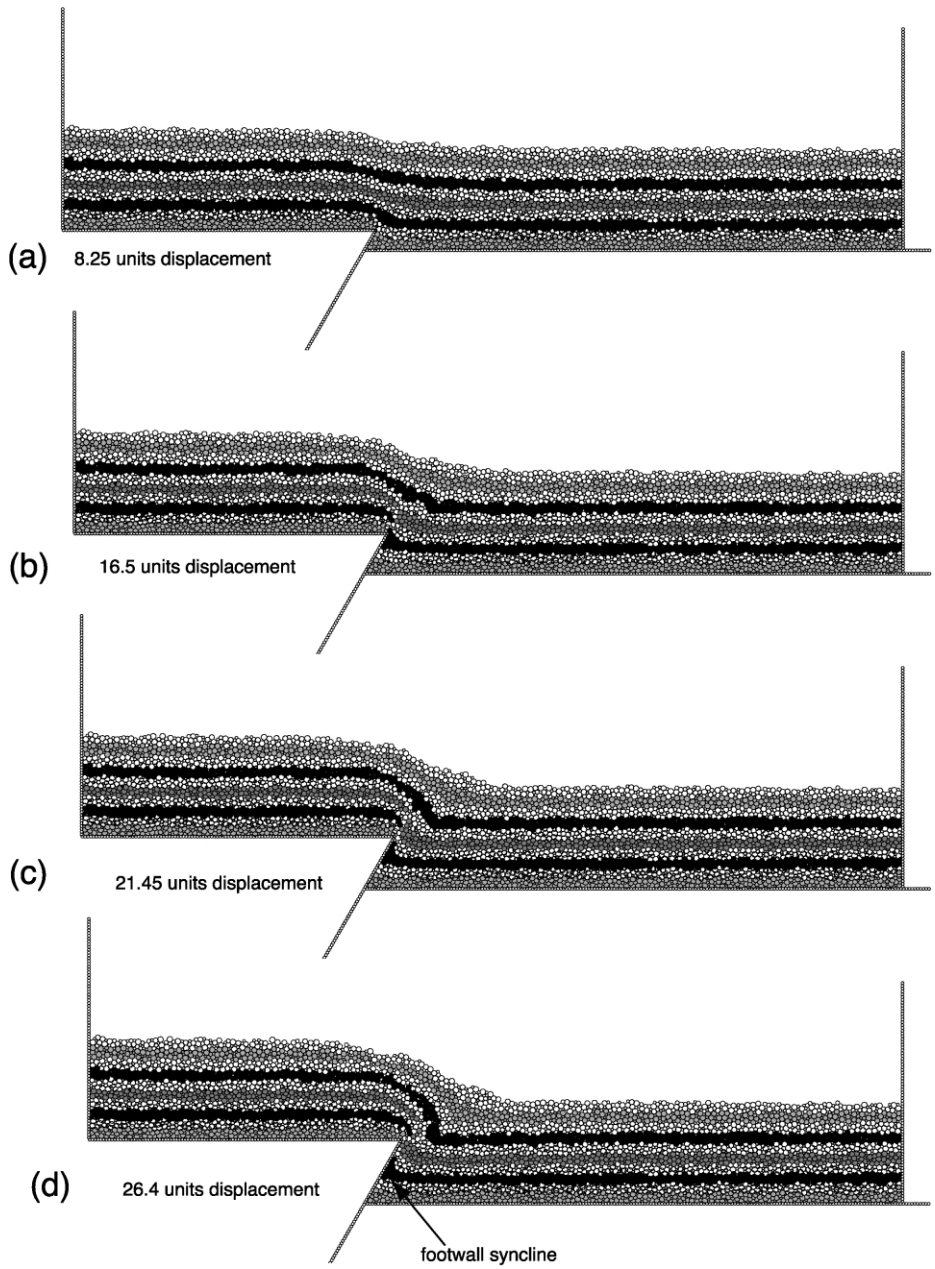

Fig. 6. Sequential evolution of a model with a basement fault dip of 60°. Configuration of the model is shown after (a) 330,000, (b) 660,000, (c) 858,000, and (d) 1,056,000 time steps. Total displacement applied is 26.4 units, all other parameters as in Fig. 3. For detailed methodology see text.

broader upward-widening zone of deformation (monocline) with shallower surface dips; (b) significant thinning and thickening of stratigraphic units within the monocline, and; (c) less discrete faulting or localization and limited fault propagation (compare Figs. 8 and 10 with Fig. 9). These features are particularly clear in Fig. 10 (the ultra-weak model) where the geometry of the fold developed is qualitatively similar to trishear fold geometries developed when the propagation to slip ratio (p/s) is low ($\sim$1) (cf. Erslev, 1991; Hardy and Ford, 1997). In contrast, strong cover produces a narrower zone of deformation with steeper surface dips, less marked thinning or thickening of a given stratigraphic unit, localization on a single fault, and more rapid fault propagation (qualitatively similar to trishear fold profiles where $p/s \sim 2-3$: cf. Hardy and Ford, 1997). Together, these effects result in the development of only minor footwall synclines and hanging wall anticlines in the models with 'strong' cover (Fig. 9).

The differences between strong and weak sedimentary covers are illustrated by comparison of velocity vectors resulting from different cover strengths for identical displacements. We use the total displacement between time steps 132,000 and 165,000 (0.825 units, $\sim$3% total displacement) to calculate the different velocity fields above the basement fault for the ultra-weak and strong models described above (Fig. 11a and b). The standard and weak

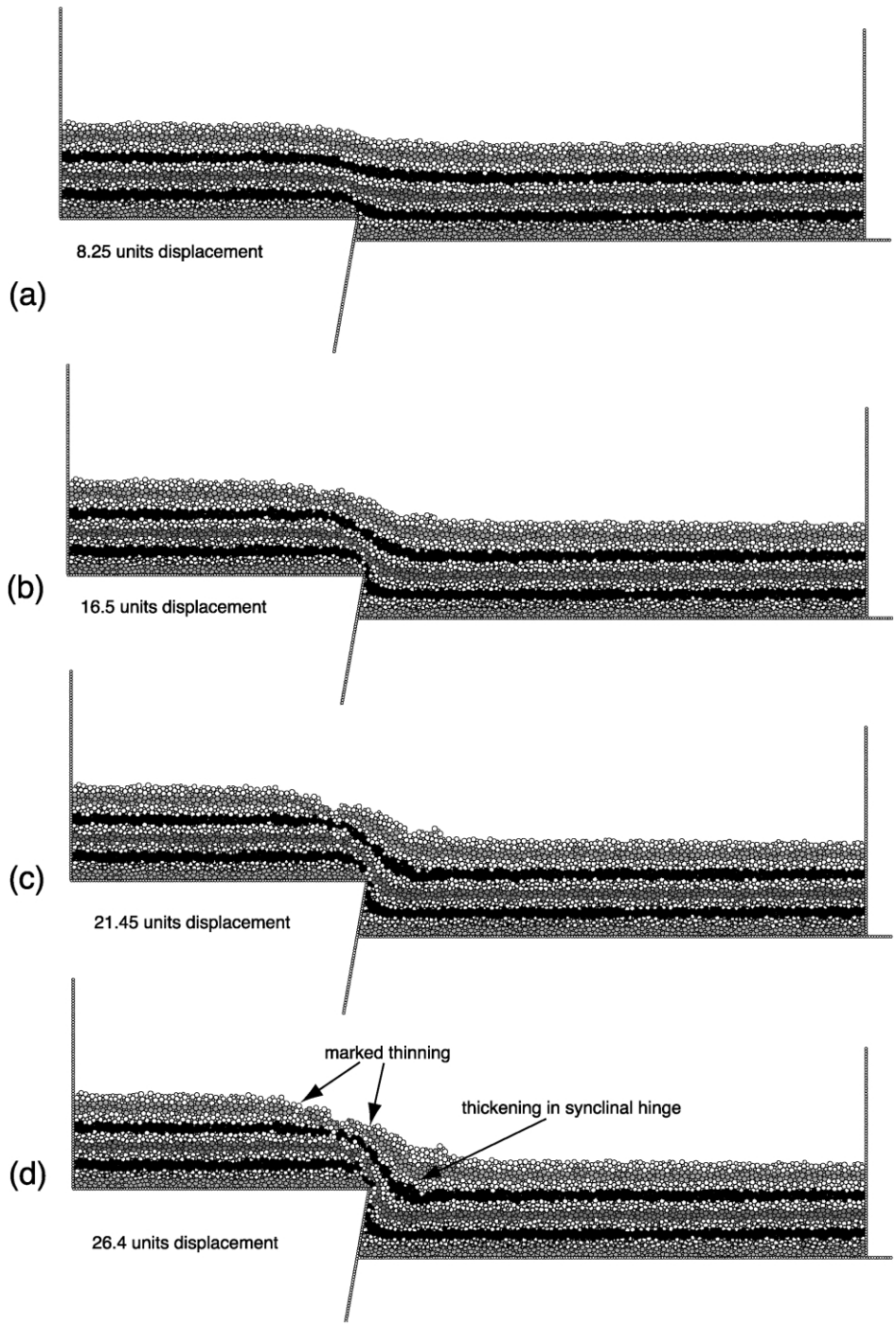

Fig. 7. Sequential evolution of a model with a basement fault dip of 80°. Configuration of the model is shown after (a) 330,000, (b) 660,000, (c) 858,000, and (d) 1,056,000 time steps. Total displacement applied is 26.4 units, all other parameters as in Fig. 3.

models have velocity fields that are transitional between the ultra-weak and strong examples. In both the ultra-weak and strong cases there is a transition from broadly rigid body translation in the hanging wall block above the fault to zero displacement in the footwall block (Fig. 11a and b). This transition occurs in an upward-widening, broadly triangular, zone, which is attached to the fault tip. The strong model shows a smooth decrease in both the magnitude and orientation of the velocity vectors from hanging wall to footwall; vectors are sub-parallel to the fault in the hanging wall and decrease to sub-parallel to the basement block in the footwall (Fig. 11b). The zone of transition has a boundary in the hanging wall that dips antithetically to the main fault at approximately 25°. All of these features are very similar to the velocity vectors which result from a simple trishear kinematic model with a linear decrease in velocity from top to bottom of the shear zone (see

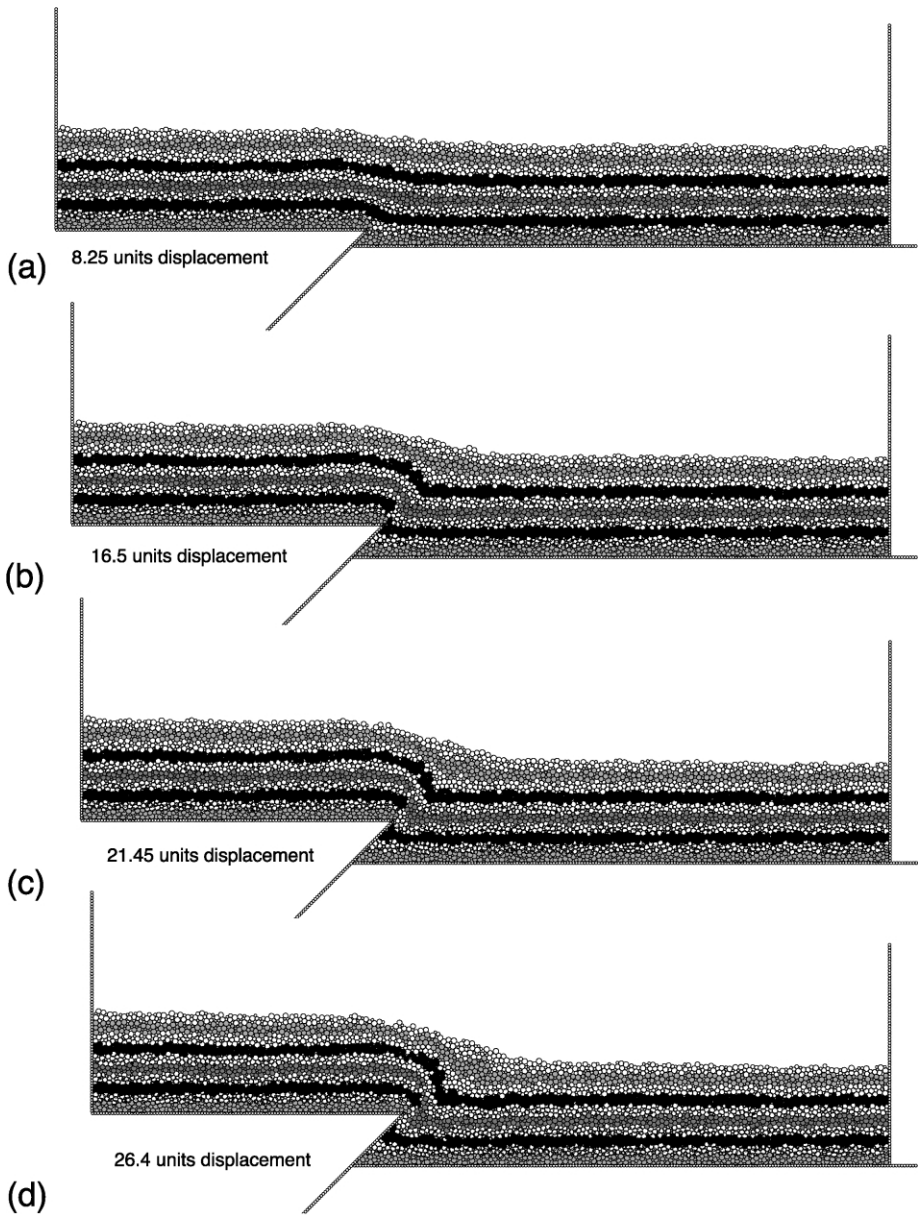

Fig. 8. Sequential evolution of a model with a basement fault dip of 45° with breaking strain reduced to 0.025*R*. Configuration of the model is shown after (a) 330,000, (b) 660,000, (c) 858,000, and (d) 1,056,000 time steps. Total displacement applied is 26.4 units, all other parameters as in Fig. 3.

Zehnder and Allmendinger, 2000). The ultra-weak model diverges from this simple pattern however; the distribution of both magnitudes and orientations of velocity vectors is much more complex (Fig. 11a), suggesting that a simple trishear model would have difficulty producing the geometry of this type of structure. Finally, for comparison, velocity vectors for the strong model between time steps 660,000 and 693,000 are shown in Fig. 11c. The effect that fault tip propagation has on velocity vectors is clearly seen here. It can also be seen that the zone of active deformation migrates with, or is attached to, the fault tip as it propagates into the cover.

4. Discussion

The discrete element model presented here attempts to predict the broad-scale features and basic characteristics of distributed deformation developed above blind contractional faults at depth. It is quite different in approach to previous numerical studies of 'forced' folding using block motion viscous or finite element mechanical models (e.g. Patton and Fletcher, 1995; Niño et al., 1998; Cardozo et al., 2002; Johnson and Johnson, 2002b). However, it reproduces many of the features seen both in analogue models and reported from outcrop and seismic studies (Withjack et al., 1990; Mitra and Islam, 1994; Gawthorpe et al., 1997). In

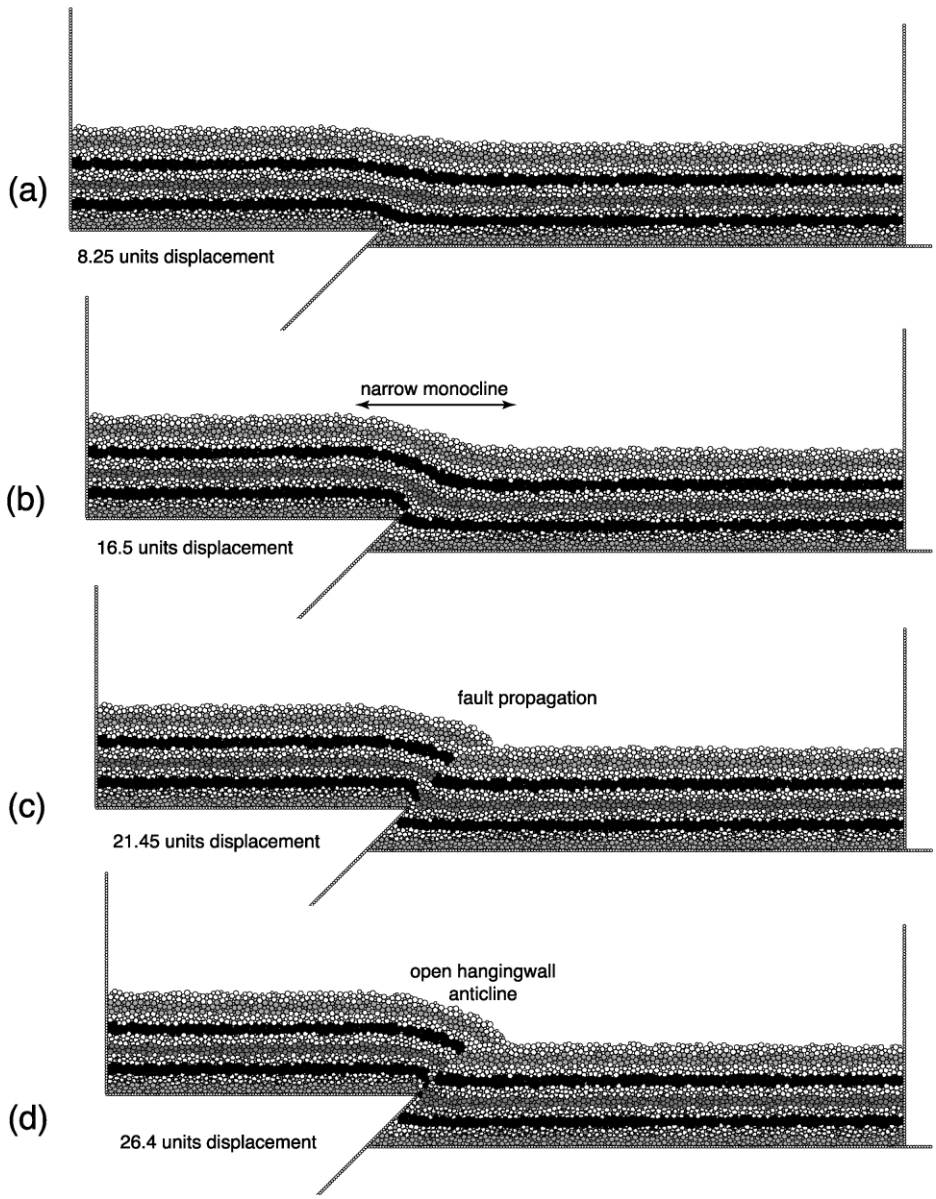

Fig. 9. Sequential evolution of a model with a basement fault dip of 45° with breaking strain increased to 0.10*R*. Configuration of the model is shown after (a) 330,000, (b) 660,000, (c) 858,000, and (d) 1,056,000 time steps. Total displacement applied is 26.4 units, all other parameters as in Fig. 3.

particular, the model successfully reproduces an upward-widening monocline (fault-propagation fold) linked to the discrete basement fault at depth. A key feature of our model, particularly noticeable in models with a strong cover, is the 'unforced' propagation of the basement fault into the cover stratigraphy. This has not been considered in previous studies of forced folding using block motion viscous or finite element mechanical models (e.g. Patton and Fletcher, 1995; Johnson and Johnson, 2002a). This localization and propagation of faults in the cover stratigraphy is a distinct advantage of our modelling approach. In our experience most forced fold structures experience fault-propagation, unless the cover stratigraphy is very weak. The propagation of the basement fault into the cover produces hanging wall anticlines and footwall synclines adjacent to the fault plane. In the strong models we see a transition from an early stage of evolution dominated by folding to a later stage of localization of deformation onto a single fault.

In an effort to better understand the controls on the geometry of fault-propagation folds associated with basement blocks, we have investigated two key parameters of our model: (1) basement fault dip; and (2) sedimentary cover strength. We find that shallow dipping basement faults produce homogenous thickening of the monocline limb while steeper faults produce contemporaneous extensional and contractional structures within the sedimentary cover. A more important effect is, that for a given fault dip, we find that weak cover strength promotes more 'ductile' macroscopic behaviour, resulting in wide zones of deformation and limited fault-propagation. Strong cover, on the

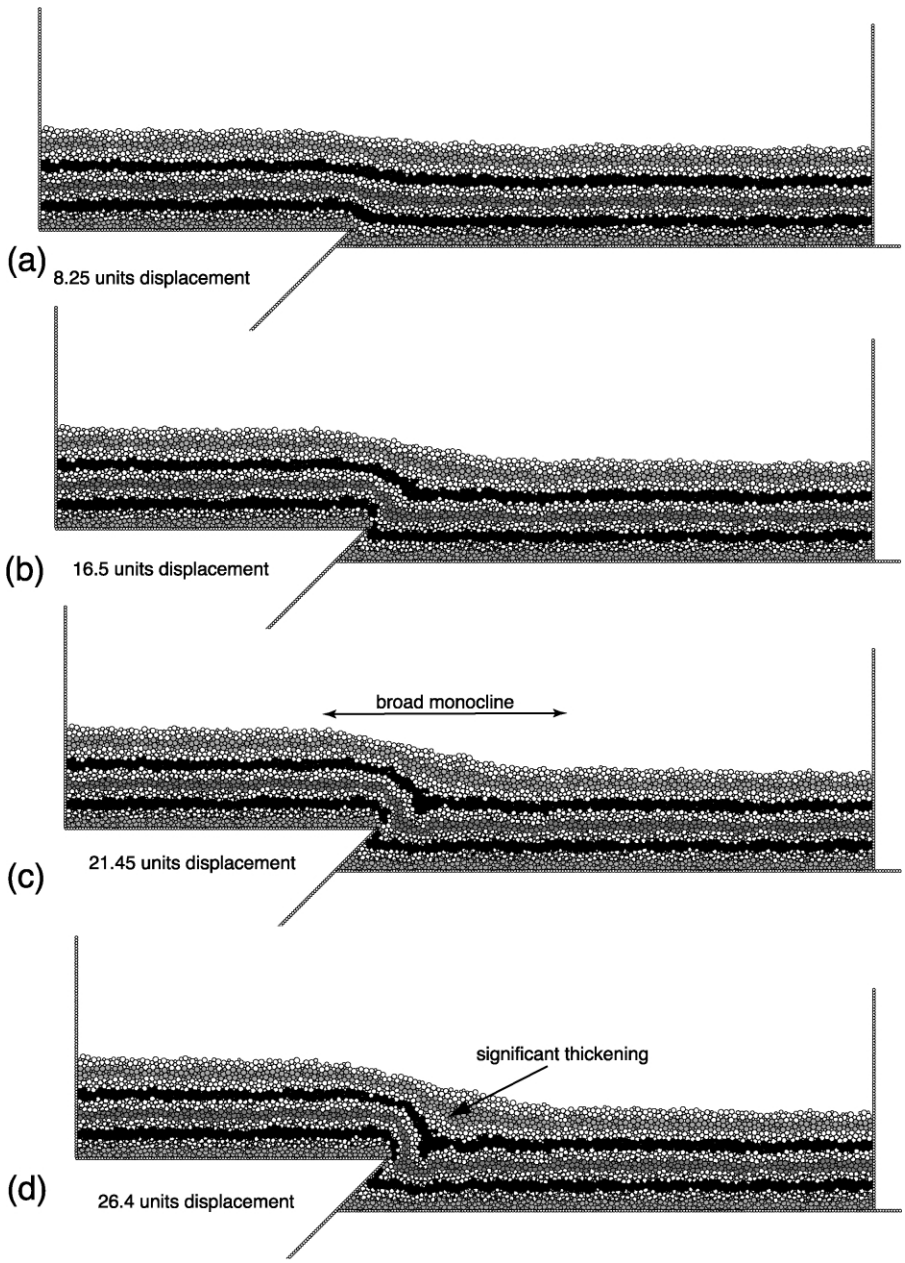

Fig. 10. Sequential evolution of a model with a basement fault dip of 45° with breaking strain decreased to 0.01*R*. Configuration of the model is shown after (a) 330,000, (b) 660,000, (c) 858,000, and (d) 1,056,000 time steps. Total displacement applied is 26.4 units, all other parameters as in Fig. 3.

other hand, produces a narrow zone of deformation and faster fault propagation. Thus the localization of faulting in our models is a key feature of strong vs. weak cover sequences. Thus we find that the propagation to slip ratio (p/s) is a gross reflection of the strength of the cover, confirming the intuitive hypothesis of Allmendinger (1998) that the p/s in the trishear model should reflect either mechanics or overpressure.

The results presented here are very similar to those predicted from the purely kinematic trishear model and its derivatives (Erslev, 1991; Hardy and Ford, 1997; Zehnder and Allmendinger, 2000). This is hardly surprising, in that the kinematic model was developed to explain the geometries of folds seen in sedimentary cover overlying basement uplifts, but does confirm that the trishear model is an adequate kinematic description of deformation in these fault systems. By definition in our models the p/s must be $\geqq 1$ as the basement block is completely undeformed. In detail the discrete element model has more small-scale faulting, bed discontinuities etc.; however, the ability of the simple kinematic model to reproduce deeper geometric configurations is encouraging. We do, however, find that velocity vectors for our ultra-weak model depart significantly from the simple assumptions built in to the trishear kinematic model.

In this study we have not investigated the influence of

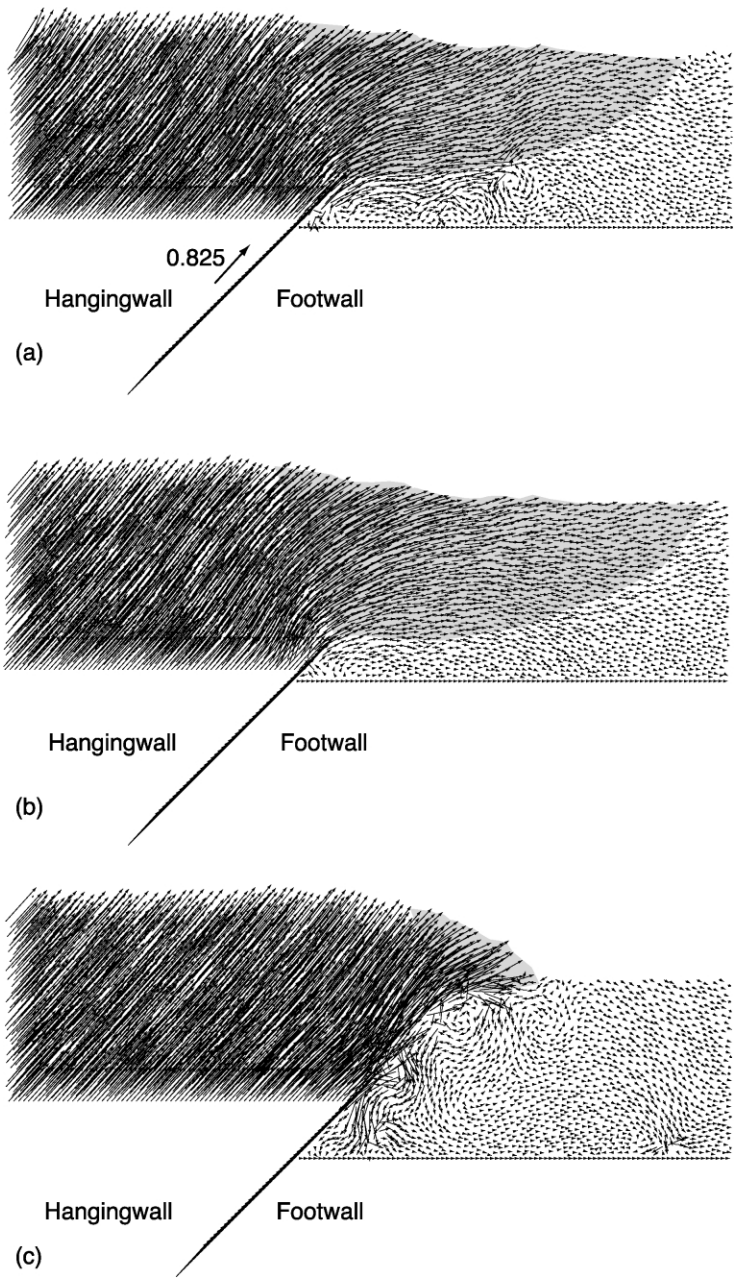

Fig. 11. Velocity vectors for the central part of the (a) ultra-weak model and (b) the strong model calculated for time steps 132,000 and 165,000. (c) Velocity vectors for the central part of the strong model calculated for time steps 660,000 and 693,000. Velocity vectors are exaggerated by a factor of 10. Approximate transition zones between hanging wall and footwall velocity vectors are indicated in grey.

strength variations (anisotropy) within the cover on the nature of fold development and fault-propagation. We would expect that mechanically-layered cover stratigraphy would promote the development of more kink-like geometries (cf. Narr and Suppe, 1993; Niño et al., 1998; Johnson and Johnson, 2002b). In principle, particle sizes and inter-particle bonding relationships of the system can be changed to investigate the effect of interlayering of weaker/stronger beds and bed-parallel slip on the relationship between faulting and folding. There are, however, computational limitations on the number of particles that can be used to describe a cover sequence. In addition, linkage with other faults both in the plane of tectonic transport and perpendicular to it (e.g. Burbank et al., 1999) is a key process by which a fault tip line propagates. Such interaction and linkage is not presently included in the modelling scheme.

Finally, we have concentrated upon the structures seen in strata laid down before deformation occurs. Growth strata, when present (e.g. Gawthorpe et al., 1997), allow further constraints to be placed upon the evolution of contractional and extensional fault-propagation folds (e.g. Ford et al., 1997; Strayer et al., 2002). The addition of growth strata to the discrete element model described herein is a straightforward task and is the subject of ongoing research.

5. Conclusions

A 2D discrete element model of contractional fault-propagation folding has been developed. The model links discrete faulting at depth to deformation of an initially unfaulted cover stratigraphy. The model reproduces many of the features seen both in analogue models and reported from outcrop and seismic studies (Withjack et al., 1990; Stewart et al., 1996; Gawthorpe et al., 1997). In particular the model successfully reproduces an upward-widening monocline (fault-propagation fold) linked to a discrete fault at depth. The basement fault propagates into the cover stratigraphy in strong models as a result of localization and at approximately the same angle as the basement fault. Fault-propagation produces hanging wall-synclines and footwall-anticlines adjacent to the fault plane which represent a breached monocline rather than drag against the fault plane. We have investigated the effect of the dip of the basement fault on the model, and the strength of the cover stratigraphic sequence. We find that shallow basement fault dips produce homogenous thickening of the monocline limb while steeper fault dips produce contemporaneous extensional and contractional structures within the sedimentary cover. Weak cover strength promotes cover flowage, wide zones of deformation and limited fault-propagation, whereas a strong cover produces a narrow zone of deformation and faster fault propagation. Thus, high p/s ratios in trishear models correspond to strong cover sequences whereas low p/s ratios are indicative of a weak cover. Velocity vectors in our models are similar to those predicted by the trishear kinematic model and confirm its utility in modelling the geometry of such structures.

Acknowledgments

This work has been in part funded by a University of Manchester grant to Hardy and a NERC grant to Gawthorpe. Supercomputing support from The University of Manchester CSAR is gratefully acknowledged. Reviews by Rick Allmendinger and Luther Strayer have greatly improved the content and focus of this paper. Thanks must also go to John McCloskey of the University of Ulster for his support during EF's development of the discrete element code. This work has benefited greatly from discussions with many colleagues; however, a special thanks must go to Rick Allmendinger for his open exchange of ideas, preprints and code on trishear kinematics and mechanics.

References

Allen, M.P., Tildesley, D.J., 1987. Computer Simulation of Liquids, Oxford Science Publications, Oxford.

Allmendinger, R.W., 1998. Inverse and forward numerical modeling of trishear fault-propagation folds. Tectonics 17, 640–656.

Allmendinger, R.W., Shaw, J., 2000. Estimation of fault propagation distance from fold shape: Implications for earthquake hazard assessment. Geology 28, 1099–1102.

Allmendinger, R.W., Zapata, T.R., Manceda, R., Dzelalija, F., 2002. Trishear kinematic modeling of structures with examples from the Neuquén Basin, Argentina. In: McClay, K.R. (Ed.), AAPG Thrust Tectonics Conference. American Association of Petroleum Geologists, Special Publication, in press.

Antonellini, M.A., Pollard, D.D., 1995. Distinct element modeling of deformation bands in sandstone. Journal of Structural Geology 17, 1165–1182.

Burbank, D.W., McLean, J.K., Bullen, M., Abdrakhmatov, K.Y., Miller, M.M., 1999. Partitioning of intermontane basins by thrust-related folding, Tien Shan, Kyrgyzstan. Basin Research 11, 75–92.

Cardozo, N., Bawa-Bhalla, K., Zehnder, A., Allmendinger, R.W., 2002. Mechanical models of fault propagation folds and comparison to the trishear kinematic model. Journal of Structural Geology, in press.

Cundall, P.A., Strack, O.D.L., 1979. A discrete numerical model for granular assemblies. Géotechnique 29, 47–65.

Donzé, F., Mora, P., Magnier, S.A., 1994. Numerical simulation of faults and shear zones. Geophysical Journal International 116, 46–52.

Erslev, E.A., 1991. Trishear fault-propagation folding. Geology 19, 617–620.

Erslev, E.A., Mayborn, K.R., 1997. Multiple geometries and modes of fault-propagation folding in the Canadian thrust belt. Journal of Structural Geology 19, 321–335.

Erslev, E.A., Rogers, J.L., 1993. Basement-cover geometry of Laramide fault-propagation folds. In: Schmidt, C.J., Chase, R.B., Erslev, E.A. (Eds.), Laramide Basement Deformation in the Rocky Mountain Foreland of the Western United States. Geological Society of America Special Paper 280, pp. 125–146.

Ford, M., Williams, E.A., Artoni, A., Vergés, J., Hardy, S., 1997. Progressive evolution of a fault propagation fold pair as recorded by growth strata geometries, Sant Llorenç de Morunys, SE Pyrenees. Journal of Structural Geology 19, 413–441.

Gawthorpe, R.L., Sharp, I., Underhill, J.R., Gupta, S., 1997. Linked sequence stratigraphic and structural evolution of propagating normal faults. Geology 25, 795–798.

Haneberg, W.C., 1992. Drape folding of compressible elastic layers—I. Analytical solutions for vertical uplift. Journal of Structural Geology 14, 713–721.

Haneberg, W.C., 1993. Drape folding of compressible elastic layers—II. Matrix solution for two-layer folds. Journal of Structural Geology 15, 923–932.

Hardy, S., Ford, M., 1997. Numerical modeling of trishear fault-propagation folding. Tectonics 16, 841–854.

Hardy, S., McClay, K.R., 1999. Kinematic modeling of extensional fault-propagation folding. Journal of Structural Geology 21, 695–702.

Janecke, S.U., Vandenburg, C.J., Blankenau, J.J., 1998. Geometry, mechanisms, and significance of extensional folds from examples in the Rocky Mountain Basin and Range province, USA. Journal of Structural Geology 20, 841–856.

Johnson, K.M., Johnson, A.M., 2002a. Mechanical models of trishear-like folds. Journal of Structural Geology 24, 277–287.

Johnson, K.M., Johnson, A.M., 2002b. Mechanical analysis of the geometry of forced-folds. Journal of Structural Geology 24, 401–410.

Laubscher, H.P., 1982. Die Sudostecke des Rheingrabens—ein kinematisches und dynamisches problem. Eclogae Geologicae Helvetiae 75, 101–116.

Mitra, S., Islam, Q.T., 1994. Experimental (clay) models of inversion structures. Tectonophysics 230, 211–222.

Mitra, S., Mount, V.S., 1998. Foreland basement-involved structures. American Association of Petroleum Geologists Bulletin 82, 70–109.

Mora, P., Place, D., 1993. A lattice solid model for the non-linear dynamics

of earthquakes. International Journal of Modern. Physics C 4 (6), 1059–1074.

Mora, P., Place, D., 1994. Simulation of the frictional stick-slip instability. Pure and Applied Geophysics 143, 61–87.

Narr, W., Suppe, J., 1993. Kinematics of basement-involved compressive structures. American Journal of Science 294, 302–360.

Niño, F., Philip, H., Chery, J., 1998. The role of bed-parallel slip in the formation of blind thrust faults. Journal of Structural Geology 20, 503–516.

Patton, T.L., Fletcher, R.C., 1995. Mathematical block-motion model for deformation of a layer above a buried fault of arbitrary dip and sense of slip. Journal of Structural Geology 17, 1455–1472.

Schlische, R.W., 1995. Geometry and origin of fault-related folds in extensional settings. American Association of Petroleum Geologists Bulletin 79, 1661–1678.

Scott, D.R., 1996. Seismicity and stress rotation in a granular model of the brittle crust. Nature 381 (6583), 592–595.

Sharp, I.R., Gawthorpe, R.L., Underhill, J.R., Gupta, S., 2000. Fault-propagation folding in extensional settings: examples of structural style and synrift sedimentary response from the Suez Rift, Sinai, Egypt. Geological Society of America Bulletin 112, 1877–1899.

Shaw, J.H., Shearer, P.M., 1999. An elusive blind-thrust fault beneath metropolitan Los Angeles. Science 283, 1516–1518.

Stearns, D.W., 1978. Faulting and forced folding in the Rocky Mountains foreland. In: Matthews, V., III (Ed.), Laramide Folding Associated with Basement Block Faulting in the Western United States. Geological Society of America Memoir 151, pp. 1–37.

Stewart, S.A., Harvey, M.J., Otto, S.C., Weston, P.J., 1996. Influence of salt on fault geometry: examples from the UK salt basins. In: Alsop, G.I., Blundell, D.J., Davison, I. (Eds.), Salt Tectonics. Geological Society Special Publication 100, pp. 175–202.

Strayer, L.M., Erickson, S.G., Suppe, J., 2002. Influence of growth-strata on the evolution of fault-related folds: distinct element models. In: McClay, K.R. (Ed.), AAPG Thrust Tectonics Conference. American Association of Petroleum Geologists, Special Publication, in press.

Withjack, M.O., Meisling, K.E., Russell, L.R., 1988. Forced folding and basement-detached normal faulting in the Haltenbanken area, offshore Norway. American Association of Petroleum Geologists Bulletin 72, 259.

Withjack, M.O., Olson, J., Peterson, E., 1990. Experimental models of extensional forced folds. American Association of Petroleum Geologists Bulletin 74, 1038–1054.

Zehnder, A.T., Allmendinger, R.W., 2000. Velocity field for the trishear model. Journal of Structural Geology 22, 1009–1014.